Atmos. Meas. Tech. Discuss.,
doi:10.5194/amt-2019-11-AC1, 2019

Atmospheric Measurement Techniques Discussions

Interactive comment on "Evaluation of ambient ammonia measurements from a research aircraft using a closed-path QC-TILDAS spectrometer operated with active continuous passivation" *by* Ilana B. Pollack et al.

Ilana B. Pollack et al.

ipollack@rams.colostate.edu

Received and published: 15 April 2019

We greatly thank Anonymous Reviewer #2 for their time and effort to provide detailed specific comments for this manuscript, which have greatly improved the accuracy and clarity of this work. Below is our response to each of the reviewer's specific comments.

We note the temperature of the aircraft cabin on Page 1, Line 17 (in the abstract) by adding "(e.g., average aircraft cabin temperatures expected to exceed 30 °C during summer deployments)".

We have amended Sect. 2.2.2 on Page 4, Line 26 and figure 1 with a more detailed description of the inertial inlet. This section now reads as: "The NH3 QC-TILDAS detector is typically operated with a heated inertial inlet positioned upstream of the spectrometer to provide filter-less separation of particles >300 nm from the sample stream, as shown in Fig. 1a. Coupling an inertial inlet with a QC-TILDAS has been well established following several laboratory and ground-based field experiments (Ellis et al., 2010; Ferrara et al., 2012; Tevlin et al., 2017; von Bobrutzki et al., 2010; Zöll et al., 2016). The inertial inlet is described in detail by Ellis et al. (2010) and Roscioli et al. (2016). Briefly, the inertial inlet used in these experiments consists of a quartz tube (12.7 mm o.d., 10.4 mm i.d.) with an integral, conical-shaped critical orifice roughly 1 mm in diameter positioned at about half the length of the tube, as shown in Fig. 1a. After passing through the orifice, gas (and particulates) are accelerated to a higher speed at a lower pressure (between 40 and 100 Torr) through the latter half of the 12.7 mm quartz tube, and then pass into a second quartz tube (25.2 mm o.d., 22.2 mm i.d.) that is sleeved around the 12.7 mm tube. The sample flow is split into two branches with approximately 90% of the total flow through the critical orifice (denoted by the blue arrow in Fig. 1a) being forced to make an 180 degree turn around the edge of the 12.7 mm tubing to continue to the spectrometer, and the other 10% (denoted by the orange arrow in Fig. 1a) being dumped via the straight section of 25.2 mm tube into the main pumping system. The inertia of particles with aerodynamic diameters greater than ∼300 nm is too large to follow the gas stream around the 180 degree turn, thereby forcing the particles into the 10% of the flow stream that is directed to the pumping system. Ellis et al. (2010) reported that the inertial inlet, which acts like a form of virtual impactor, removes more than 50% of particles larger than 300 nm. A tee positioned immediately upstream of the critical orifice allows for pressure measurements using a baraton transducer (range 0-1000 Torr), which is used in determining the sample flow rate, and an auxiliary draw that allows the dead volume around the base of the conical-shaped critical orifice to be actively flushed. The flow rate of the auxiliary draw ranges from 160 to 500 sccm with changes in ambient pressure at the inlet tip. The inertial

inlet is housed in a fiberglass enclosure, with the inside of the enclosure maintained at 40 degrees C."

We agree with the reviewer that there is some confusion about how the uncertainty in the calibration source is determined in Sect. 2.3 on Page 6, Line 46. The text has been updated to include the uncertainties of the individual reported values from Froyd and Lovejoy (2012) (4.67 $\pm$ 0.08 x 10-18 cm2), Chen et al. (1998) (4.7 $\pm$ 0.5 x 10-18 cm2) and Cheng et al. (2006) (4.7 $\pm$ 0.5 x 10-18 cm2). Also, following careful consideration of the reviewer's comment, we now utilize the weighted average and associated propagated uncertainty of 4.7 $\pm$ 0.1 x 10-18 cm2 as a more appropriate treatment for combining the cross section values from the literature. The weighted mean absorption cross section utilized here is in agreement within the uncertainties with the value reported by Neuman et al. (2003) (e.g., 4.4 $\pm$ 0.3 x 10-18 cm2). We have also modified the text in Sect. 2.3 to clarify that the $\pm$2% uncertainty in the weighted mean of the absorption cross section has been factored into the total estimated uncertainty ($\pm$7%) associated with the NH3 calibration source used in these experiments. Further, with only a $\pm$2% uncertainty on the weighted average of the updated cross sections, the uncertainty in the absorption cross section is no longer the dominating factor in the total uncertainty of the calibration source using the NOAA UV optical absorption system. The $\pm$7% uncertainty in the calibration source is factored into the overall instrument uncertainty (e.g., 200 pptv $\pm$ 12%), as described in Sect. 4.1. We have amended this portion of Sect 2.3 as follows: "In this work, we refine the uncertainty of the NOAA calibration of the emission rate of the permeation device used in these experiments by utilizing more recent assessments of the NH3 absorption cross section reported in the literature. Here, we use a weighted average of the NH3 absorption cross sections reported by Froyd and Lovejoy (2012) (4.67 $\pm$ 0.08 x 10-18 cm2), Chen et al. (1998) (4.7 $\pm$ 0.5 x 10-18 cm2) and Cheng et al. (2006) (4.7 $\pm$ 0.5 x 10-18 cm2). The weighted mean utilized here (4.7 $\pm$ 0.1 x 10-18 cm2) is in agreement within the uncertainties with the value reported by Neuman et al. (2003) (e.g., 4.4 $\pm$ 0.3 x 10-18 cm2). Combining in quadrature the $\pm$2% uncertainty associated with the weighted mean of the absorption

cross section, the $\pm$2.5% uncertainty in the stability of the permeation device between pre- and post-project calibrations with the NOAA UV optical absorption system, and a conservative estimate of $\pm$6% for other sources of uncertainty associated with the NOAA calibration system, we determine a total estimated uncertainty of $\pm$7% for the emission rate of the permeation device used in these experiments."

The size of the critical orifice ($\sim$1 mm) has been added to Sect. 2.2.2 on Page 7, line 4-7.

We too had considered in our initial analyses whether a triple exponential fit would work better for the time profiles shown in Fig. 5. Indeed, triple exponential fits do generate a more reasonable fit of the time profiles. However, in Section 4.3, we elected to report the results of bi-exponential fits in the original manuscript for the following reasons: 1) there is more physical basis for relating a bi-exponential fit to the experiments conducted in this work, 2) the results of a bi-exponential fit could be directly compared to similar results reported by Ellis et al. (2010) and Roscioli et al. (2016), and 3) the coefficient associated with the third time constant (A3) was <5% on average of the sum of the coefficients (e.g., [A3/(A1 + A2 + A3)]) and <23% on average of the sum of the coefficients associated with the latter two time constants (e.g., [A3/(A2 + A3)]). All the same, we agree that this discussion about the possibility of a triple exponential fit does have merit in this manuscript, and thus we have added the following discussion to the end of Sect. 4.3: "Indeed, a triple exponential decay with the functional form shown in Eq. (2): y= y_0+A_1 exp((-(t-t_0))/τ_1)+A_2 exp((-(t-t_0))/τ_2)+A_3 exp((-(t-t_0))/τ_3) produces better fits to the time profiles shown in Fig. 5. A triple exponential fit might have physical meaning in terms of the instrument time response if there is more than one time constant associated with the gas exchange rate through the sample flow pathway or if there is more than one time constant associated with the interaction of NH3 molecules with the sampling surfaces. In the case of multiple time constants associated with the gas exchange rate, it is possible that different residence times could arise from the different pressure regimes of the sample flow pathway (e.g.,

the portion of the sample flow path at ambient pressure upstream of the critical orifice in the inertial inlet versus the portion of the sample flow path downstream of the critical orifice at pressures between 40 and 100 Torr). In the case of NH3 molecules interacting with the sampling surfaces, additional time constants could be related to differing levels of cleanliness along the sample flow path. For example, inlet tubing and components were cleaned/replaced following contamination, but the optical cell in the QC-TILDAS was not; thus, more than one time constant might be most plausible, especially for the "typical" and "contaminated" time profiles that were collected following contamination. All the same, we elect to report the results of the bi-exponential fits in this work for the following reasons: 1) there is more physical basis for relating a bi-exponential fit to the passivation experiments conducted in this work, 2) the results can be directly compared to the results of bi-exponential fits for similar instrumentation reported by Ellis et al. (2010) and Roscioli et al. (2016), and 3) the coefficient associated with the third time constant (A3) is small (e.g., A3 is <5% on average of the sum of the coefficients (e.g., [A3/(A1 + A2 + A3)]) and <23% on average of the sum of the coefficients associated with the latter two time constants (e.g., [A3/(A2 + A3)])."

Figure 5 has been updated with symbols for the data and solid lines for the fits according to the reviewer's suggestion.

The phrase "for the instruments as configured here" has been added to the text on Page 15, Line 19.

Figure 1a, its figure caption, and relevant parts of Sect. 2.2.3 have been updated with the i.d of the PFA tubing used, the size of the critical orifice in the inertial inlet, and the temperature the inertial inlet. In general, 3/8" o.d., $\frac{1}{4}$" i.d. PFA tubing is used for the sample flow path. In terms of tubing lengths, we had intended to indicate that the full length of the sample flow path from the inlet tip to the inertial inlet is 107 cm. We agree that the current description of the inlet lengths is confusing and may not have been accurately labelled in the original version of the manuscript; therefore, we have modified Fig. 1a and Sect. 2.2.3 to clarify. The caption for Fig. 1 now reads as: "(a)

Schematic of the instrument as configured for flight on the NSF/NCAR C-130 aircraft. The sample flow path (blue arrows) starts at the inlet tip, which is a short piece of 3/8" o.d., $\frac{1}{4}$" i.d. PFA tubing that protrudes slightly from the face of the aircraft inlet strut. A PFA injection block (1/4" i.d.) housed inside the aircraft inlet strut allows calibration gases and passivant to be added to the sample stream within a few centimetres of the inlet tip. A 71-cm length of 3/8" o.d., $\frac{1}{4}$" i.d. PFA tubing then directs ambient air into a quartz inertial inlet where particles >300 nm are separated from the sample stream, and a 36-cm length of 3/8" o.d., $\frac{1}{4}$" i.d. PFA tubing directs the sample flow from the inertial inlet to the QC-TILDAS detector. The particle-rich stream is pumped away (orange arrows). The sample flow path is heated to 40 ËŽC where possible to minimize interactions of NH3 with sampling surfaces. The sample flow path is purged overnight in the reverse flow direction with 40 sccm of N2 injected near the pressure control valve. A 0-1000 Torr range baratron (denoted as P) measures pressure just upstream of the critical orifice in the inertial inlet for active continuous determination of the sample flow rate. An auxiliary draw acts to flush the dead volume formed near the base of the conical-shaped critical orifice in the inertial inlet. (b) Solid model of the QC-TILDAS vibration isolation mounting plate. (c) Photograph of the QC-TILDAS mounted to the vibration isolation plate while installed aboard the C-130 aircraft. (d) Photograph of the impinger used for active continuous passivant addition."

According to the reviewer's suggestions, Figure 2 has been updated to also include a lower right axis in ppt, and both of the lower panels of the figure have been updated to display the same scale on the the right and left y-axes. The caption now reads as: "10-Hz measurements collected while overblowing NH3-free air at the inlet tip (a) in flight in the boundary layer near 1.4 km AGL and (b) on the ground in the laboratory. Upper traces represent the raw 10-Hz data collected; lower traces depict the Allan variance in ppb2 (left axis) and Allan deviation in ppt (right axis) of the corresponding data set. An offset was applied to the Allan variance in panel (a) to reflect the vibration applied to the laser objective to reduce motion sensitivity in flight; the vibration was not applied during laboratory tests depicted in panel (b)."

Figure 1

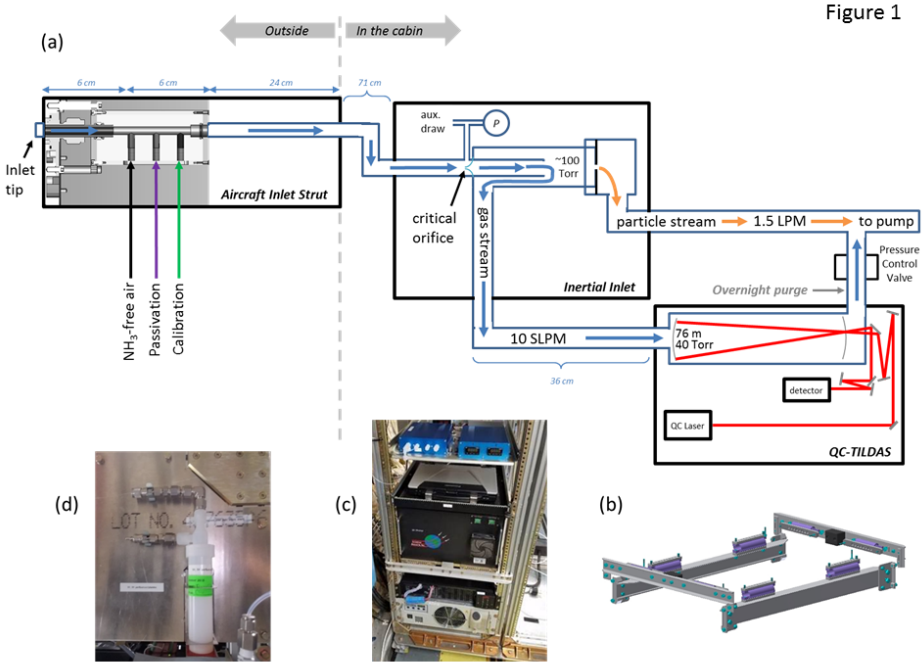

Fig. 1.

Figure 2

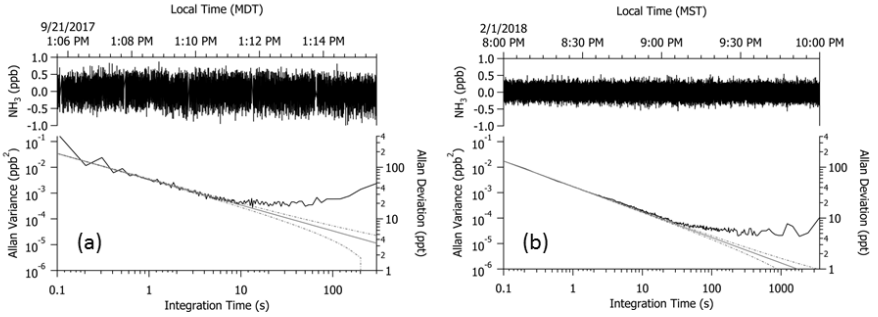

Fig. 2.

Figure 5

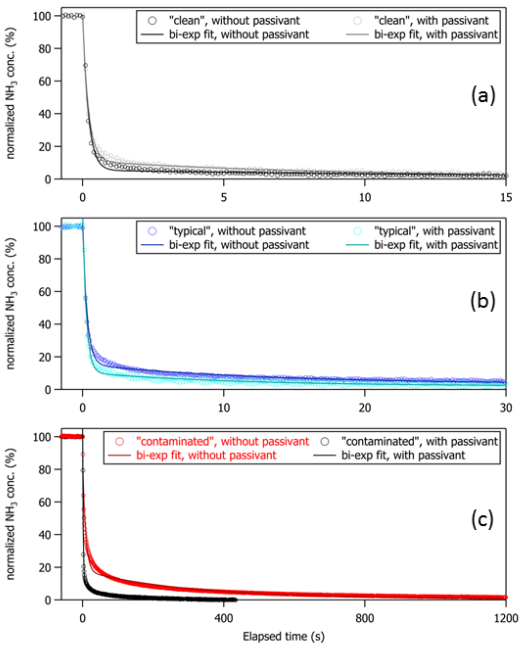

Fig. 3.